High Precision, Electrochemical Detection of Reversible Binding of Recombinant Proteins on Wide Bandgap GaN Electrodes Functionalized with Biomembrane Models

Nataliya Frenkel, Jens Wallys, Sara Lippert, Jörg Teubert, Stefan Kaufmann, Aparna Das, Eva Monroy Martin Eickhoff and Motomu Tanaka**

We report a novel hybrid charge sensor realized by the deposition of phospholipid monolayers on highly doped *n*-GaN electrodes. To detect the binding of recombinant proteins with histidine-tags, lipid vesicles containing chelator lipids were deposited on GaN electrodes pre-coated with octadecyltrimethoxysilane monolayers. Owing to its optical transparency, GaN allows the confirmation of the fluidity of supported membranes by fluorescence recovery after photo-bleaching (FRAP). The electrolyte-(organic) insulator-semiconductor (EIS) setup enables one to transduce variations in the surface charge density ΔQ into a change in the interface capacitance ΔC_p and, thus, the flat-band potential ΔU_{FB}. The obtained results demonstrate that the membrane-based charge sensor can reach a high sensitivity to detect reversible changes in the surface charge density on the membranes by the formation of chelator complexes, docking of eGFP with histidine tags, and cancellation by EDTA. The achievable resolution of $\Delta Q \geq 0.1$ μC/cm^2 is better than that obtained for membrane-functionalized *p*-GaAs, 0.9 μC/cm^2, and for ITO coated with a polymer supported lipid monolayer, 2.2 μC/cm^2. Moreover, we examined the potential application of optically active InGaN/GaN quantum dot structures, for the detection of changes in the surface potential from the photoluminescence signals measured at room temperature.

1. Introduction

Functional immobilization of biological systems on the surface of solid-based devices is an interdisciplinary challenge towards the creation of novel hybrid sensor materials. The application of advanced semiconductor technology can offer a great advantage, since specific functions of biomacromolecules can be translated into electronic readouts of semiconductor devices.[1] Combination of supported membranes with solid surfaces is a promising strategy to provide a natural environment for the immobilization of proteins under non-denaturing conditions and in well-defined orientation.[2]

To date, many studies demonstrated several prototypes of novel sensor platforms based on chemically functionalized Si nanowires,[3] carbon nanotubes,[4] and two-dimensional electron gases.[5] Organic thin films, such as organic transistors,[6] polymer films, have been proposed as sensor materials to detect changes in pH,[7] metal ions,[8] and carbon monoxide.[9] However, despite of successful demonstrations of the proof of principle, the quantitative control of density and orientation of the functional molecules and the suppression of noise still remain challenging. A promising strategy to overcome the abovementioned problems is to utilize self-assembly of lipid membranes. As demonstrated previously, hydrophilic surfaces of oxides[10] and polymer supports[11] can readily be coated with lipid membranes, and the fluid nature of "supported lipid membranes" realizes the self-healing of local defects.[12] Owing to high electric resistance of lipid membranes (up to MΩcm^2),[10b,13] it is possible to minimize the noise (leak) current. Supported lipid membranes can be functionalized with various functional proteins connected to specific "tags (histidine, biotin, etc.)". The average distance between the membrane-coupled proteins $\langle d \rangle$ can be controlled in nm accuracy by the molar fraction χ of anchor lipids, by assuming the mean molecular area of one lipid molecule A to be 65 Å^2[2b,14] $\langle d \rangle \sim \sqrt{A/\chi}$.

For the semiconducting solid-state part of the hybrid structures, Si-based devices with functionalized Si/SiO_2 surfaces have been most commonly used for the detection of cellular[15]

N. Frenkel, Dr. S. Kaufmann, Prof. M. Tanaka
Physical Chemistry of Biosystems
Institute of Physical Chemistry
University of Heidelberg
69120, Heidelberg, Germany
E-mail: tanaka@uni-heidelberg.de

N. Frenkel, Prof. M. Tanaka
Cell Biophysics Lab
Institute of Toxicology and Genetics
Karlsruhe Institute of Technology
76021, Karlsruhe, Germany

Prof. M. Tanaka
Institute for Integrated Cell-Material Science (WPI iCeMS)
Kyoto University
6068501, Kyoto, Japan

J. Wallys, S. Lippert, Dr. J. Teubert, Prof. M. Eickhoff
I Physikalisches Institut
Justus-Liebig-Universität Gießen
Heinrich-Buff-Ring 16 35392 Gießen, Germany
E-mail: Martin.Eickhoff@exp1.physik.uni-giessen.de

Dr. A. Das, Dr. E. Monroy
CEA Grenoble, INAC/SP2M/NPSC
17 rue des Martyrs F-38054 Grenoble 9, France

DOI: 10.1002/adfm.201400388

and protein functions.[10b] However, Si-based devices have fundamental drawbacks concerning bandgap engineering and suffer from instability in physiological buffers due to ion diffusion into SiO_2.[16] GaN is a wide bandgap semiconductor (i.e. transparent to visible light) that is advantageous over commonly used Si-based devices due to the excellent chemical/electrochemical stability[5c,17] over broad frequency windows. Furthermore, GaN can be alloyed with In and/or Al to vary the bandgap and realize complex semiconductor heterostructures.

On the other hand, there have been only a couple of studies on the biofunctionalization of GaN such as immobilization of penicillinase on GaN surfaces modified with an aminopropyltriethoxysilane monolayer,[18] deposition of planar lipid bilayers (supported membranes) on gallium nitride (GaN) electrodes[19] and formation of amine groups on the surface of GaN.[20]

In this study, we deposited phospholipid monolayers on *n*-GaN electrodes, which are functionalized with octadecyltrimethylsilane (ODTMS) monolayers. The whole interface can be treated as an analogue of electrolyte-insulator-semiconductor (EIS) structures, so that variations in the surface potential can be detected as changes in the semiconductor space charge capacitance and, thus, the flat band potential. To modify the surface charge density of the lipid membranes reversibly, we incorporated chelator lipids in defined ratios into the supported monolayer which can form chelator complexes with divalent metal ions and couple green fluorescence proteins with histidine tags (**Scheme 1**). We propose that our setup, in combination with semiconductor technology, can serve as a reversible platform for highly sensitive detection of protein binding. Furthermore, we demonstrate optical readout of a membrane-based charge sensor using advanced substrates/electrodes with optically active InGaN quantum dots (QDs) embedded in planar GaN matrix material.[21] The details of the obtained results are described in the following sections.

2. Results and Discussion

Prior to the surface functionalization, the surface roughness of the highly Si-doped *n*-GaN layers was determined by AFM. The RMS roughness of all investigated samples was below 1.2 nm. A low surface roughness is necessary since (1) rough surfaces frequently create defects in silane monolayers and in the deposited lipid membranes, and (2) impedance spectra of electrodes with higher RMS roughness cannot be interpreted using ideal equivalent circuit models.[22]

2.1. Electrochemical Characterization of Lipid Monolayer on GaN

In a first step, the electrochemical properties of bare GaN electrodes were analyzed by impedance spectroscopy at U_{Bias} = 0 V and f = 50 mHz – 50 kHz (**Figure 1**a, black). In contrast to GaAs electrodes,[23] GaN exhibited no sign of electrochemical degradation at U_{bias} = 0–900 mV. In general, the impedance spectra of semiconductor electrodes in the presence and absence of surface layers can be fitted with equivalent circuit models (Figure 1b). According to our previous reports,[19] we fitted the impedance spectrum of bare GaN with model A, which consisted of the serial resistance R_0, accounting for the Ohmic behavior of electrolyte and contacts, the interface capacitance C_P and the interface resistance R_P. One has to note that the interface capacitance C_P included the capacitance of the

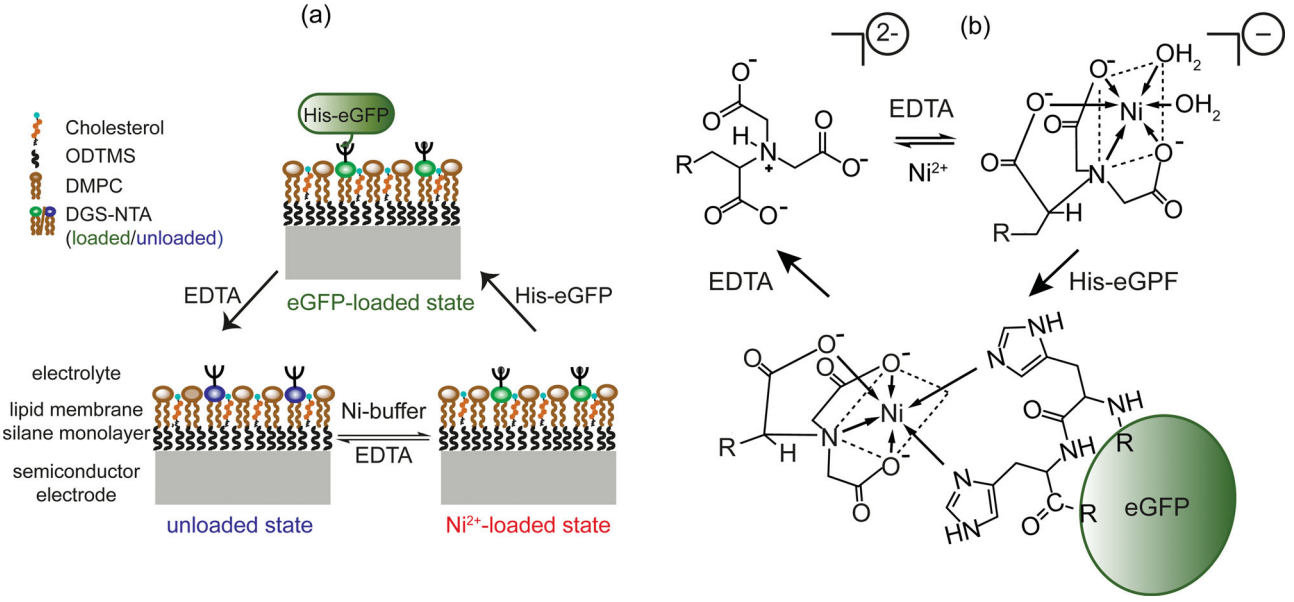

Scheme 1. (a) Schematic of reversible binding/unbinding of histidine-tagged recombinant proteins to the membrane-based charge sensor as an electrolyte-insulator-semiconductor (EIS) setup, changes in the surface potential can be detected as changes in semiconductor space charge capacitance C_{SC} and, thus, the flat band potential U_{FB}. (b) Change in the molecular conformation and net charge per molecule due to reversible binding/unbinding of histidine-tagged GFP.

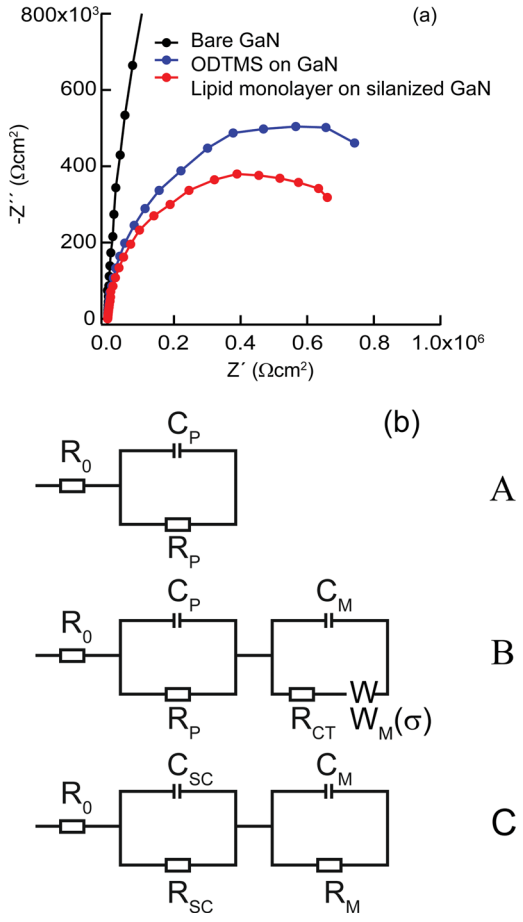

Figure 1. (a) Impedance spectra (Nyquist plot) of GaN electrodes at U_{Bias} = 0 mV: bare GaN (black), GaN before (blue) and after (red) the deposition of a lipid monolayer. (b) Equivalent circuit models used to fit the impedance spectra: Model A consists of the resistance of electrolyte and ohmic contact R_0, interface capacitance C_P and interface resistance R_P; Model B includes Warburg element W_M, the charge transfer resistance R_{CT} and a membrane capacitance C_M, Model C contains an additional ideal RC element to model the resistance R_M and the capacitance C_M of the supported membrane without Warburg element W_M.

Gouy-Chapman-Stern layer (C_{GCS}),[24] and the space charge capacitance of the semiconductor C_{SC}. Our experimental system also implies that the capacitive contribution from the surface states C_{SS}[23b,25] can be neglected, since the bias potential is far away from the flatband potential U_{FB}[26] and C_{SS} cannot be estimated quantitatively when $C_{SS}/C_{SC} < 0.1$, as previously reported.[23b,27] Thus, the interface capacitance C_P is dominated by the space charge capacitance C_{SC}. The best fit results yield $R_0 = 918\ \Omega$, $R_P = 25\ M\Omega cm^2$ and $C_P = 0.87\ \mu F cm^{-2}$.

In the next step, the impedance spectra after the deposition of ODTMS (Figure 1a, blue) and lipid monolayer (Figure 1a, red) were collected. In case of semiconductor electrodes coated with organic layers, the choice of equivalent circuit models depended on the topographic roughness and surface coverage. For example, GaAs electrodes coated with monolayers of alkylthiols[25,28] and biphenylthiols[29] could be represented by model A, as highly smooth organic monolayers with RMS roughness of 3–5 Å act as continuous dielectric layers. In contrast, ITO electrodes coated with ODTMS monolayers[30] were well characterized with model B, which includes an additional set of circuit elements based on charge transfer resistance R_{CT}, membrane capacitance C_M, and Warburg impedance W_M. In fact, a Warburg impedance in model B was used to describe the diffusion of ions across other organic monolayers[31] on metal and semiconductor electrodes. However, the application of W_M to characterize the diffusion across a layer with a finite thickness is only valid, if the distance between the diffusion pathways is small enough to allow an overlap of their spherical diffusion layers. Despite of the high surface coverage ($\Theta \sim 99.8\%$), ODTMS monolayers were not able to heal the intrinsic roughness of ITO electrodes (RMS ~ 2.6 nm) prepared by cluster deposition.[30]

In this study, the impedance spectra after the deposition of ODTMS (Figure 1a, blue) and lipid monolayers (Figure 1b, red) can be well fitted with model A, yielding the resistance and capacitance of interfaces after the deposition of ODTMS: $R_{p(ODTMS)} = 23\ M\Omega cm^2$, and $C_{p(ODTMS)} = 0.84\ \mu F cm^{-2}$, respectively.

Following our previous studies on lipid monolayers on ITO and GaAs, we analyzed the impedance spectra after the monolayer deposition (Figure 1a, red) with model B. This allows for the calculation of the electrochemical properties of lipid monolayers; $R_{CT(lipid)} = 2.7\ k\Omega cm^2$, $W_M = 0.29\ M\Omega cm^2$, and $C_{M(lipid)} = 0.70\ \mu F cm^{-2}$ ($\chi^2 = 0.11$), respectively. In contrast, we found a larger fitting error ($\chi^2 = 0.52$), when we fitted the results without Warburg impedance (model C). It is noteworthy that the diffusion barrier capability of the membrane against the diffusion of ions is not represented by R_{CT} but by W_M. The Warburg impedance $W(\omega)$ is given as a function of frequency ω and Warburg parameter σ:

$$W(\omega) = \frac{(\sigma + 1/\sigma)}{\sqrt{\omega}} \quad (1)$$

where

$$\sigma = \frac{4RT}{\sqrt{2}n^2F^2A\rho}\frac{1}{\sqrt{D}} \quad (2)$$

A is the active electrode area, D is the diffusion constant of the ions, and ρ is the charge density at the interface. The constants R, T, n, and F are gas constant, absolute temperature, the charge of ions in the electrolyte, and Faraday constant, respectively. The diffusion constant ($D \sim 1.6 \times 10^{-4}\ \mu m^2 s^{-1}$) corresponding to the Warburg parameter σ calculated from the impedance data ($\sigma > 0.3\ M\Omega cm^2\ s^{1/2}$) is about 2–3 orders of magnitude smaller than the values reported for organic layers on indium–tin oxide (ITO) electrodes, $D \sim 10^{-2} - 10^{-1}\ \mu m^2 s^{-1}$[30] suggesting that the lipid monolayer can block the passive ion diffusion and thus the leak current across the membrane.

Figure 2 represents the kinetics of lipid monolayer formation on GaN by plotting the changes in C_M and R_{CT} with time (extracted from fits using model B). Upon the injection of vesicle suspensions, on the one hand, the membrane capacitance C_M exhibited a clear decrease, implying the deposition of a dielectric layer, and, on the other hand, the charge transfer resistance R_{CT} showed a distinct increase over time. After both values

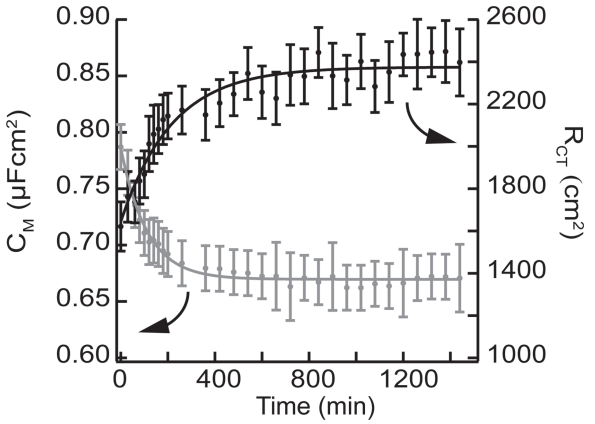

Figure 2. Kinetics of the formation of a lipid monolayer on a GaN electrode, monitored by changes in C_M and R_{CT} at U_{Bias} = 0 V. The data were empirically fitted with a first-order exponential function, resulting in the characteristic time constants τ_{Rct} = 217 min and τ_{Cm} = 103 min, respectively.

reached their saturation levels, extensive rinsing did not lead to any detectable change in the impedance spectra. The observed tendency agrees well with previous studies on the deposition of lipid monolayers on ITO[22] and GaAs[32] electrodes. The time evolution of both resistance and capacitance was empirically fitted with a first-order exponential function, yielding the characteristic time constants of τ_{Rct} = 217 min and τ_{Cm} = 103 min, respectively, which are comparable to the time constants found in studies on the lipid bilayer on GaN.[19]

In general, the self-healing of defects in lipid membranes can be achieved when the fluid nature of membranes is sustained. Therefore, we measured the lateral diffusion coefficients of lipids in supported membranes by FRAP,[33] yielding the lateral diffusion coefficient of D = 0.77 μm² s⁻¹ and the mobile fraction of 88%. This lateral diffusivity is comparable to the values on hydrophobic polymer supports, of D = 1.0–1.5 μm²s⁻¹.[34]

2.2. Capacitive Sensing of Surface Charge Density

Figure 3a represents the impedance spectra of lipid monolayers incorporating 2 mol% of DOGS-NTA measured at unloaded (blue), Ni^{2+}-loaded (red), and eGFP-loaded (green) states at U_{Bias} = 200 mV. The experimental data points can be fitted with model B (solid lines), showing distinct changes in the global shapes of the spectra.

Since a NTA groups form octahedral chelator complex with divalent metal ions e.g. Ni^{2+}, the loading and unloading of NTA result in a change in the molecular net charge by 1 e⁻.[22,35] Then, eGFP with histidine tags can be specifically immobilized on the lipid membrane by replacing H_2O ligands.[36] Finally, the complexation can be cancelled by EDTA (Scheme 1b).

Our experimental system (Scheme 1) can be generalized as electrolyte-(organic)insulator- semiconductor (EIS) system,[37] which is an analog of the metal-oxide-semiconductor (MOS) system. Therefore, variations in the membrane surface potentials due to charging of lipids or coupling of charged proteins can be detected quantitatively by monitoring changes in the semiconductor space charge capacitance C_{SC} and thus in the

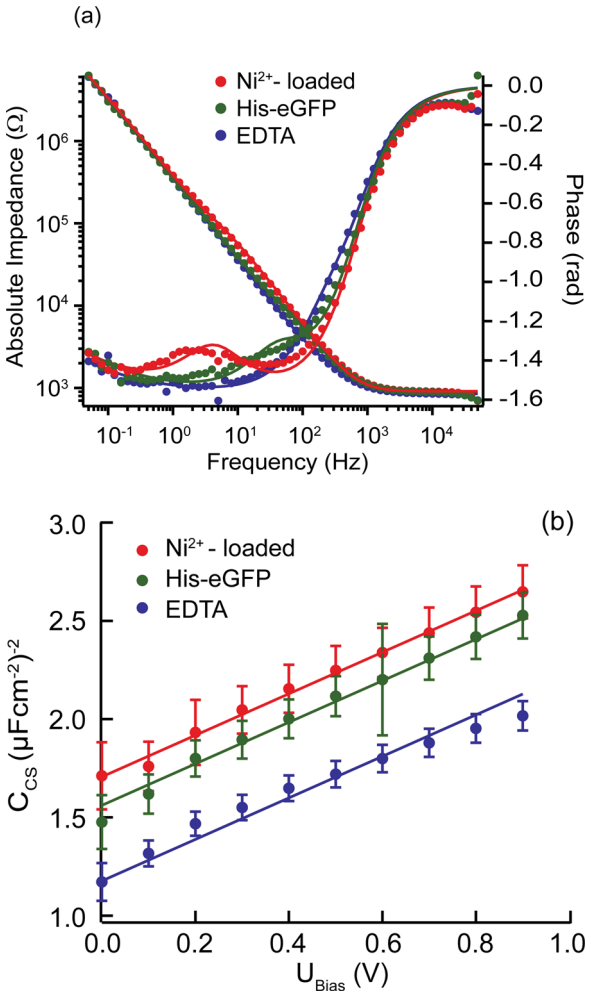

Figure 3. (a) Impedance spectra of the membrane incorporating 2 mol% of DOGS-NTA at unloaded (blue), Ni^{2+}-loaded (red), and eGFP-loaded (green) states at U_{Bias} = 200 mV, fitted with model B. (b) Mott-Schottky plot ($1/C^2_{SC}$*vs.* U_{Bias}) of the supported membranes at three different states, obtained from the interface spectra measured at 0 mV ≤ U_{Bias} ≤ 900 mV. The interface capacitance C_P is dominated by the space charge capacitance C_{SC}. The linear fitting is performed for a donor concentration of $N_D = 1.5 \times 10^{19}$ cm⁻³, determined by Hall measurements. The intercept of the extrapolated linear part with the x axis yields the flat-band potential U_{FB}. Ni^{2+}-loaded, unloaded (EDTA), and eGFP-loaded states can be distinguished by changes in the interface capacitance (Figure 4a) and the flat band potential (Figure 4b), which are summarized in Table 1.

flat band potential U_{FB} of the semiconductor. The flat band potential of the EIS can be determined by plotting $1/C_{SC}^2$ vs. bias potential U_{Bias} (Mott-Schottky analysis, Equation (3), where the extrapolation to $1/C_{SC}^2 = 0$ corresponds to U_{FB}:[38]

$$C_{SC}^{-2} = \frac{2}{\varepsilon_{SC}\varepsilon_0 e N_D}\left(U_{Bias} - U_{FB} - \frac{k_B T}{e}\right) \quad (3)$$

N_D is the donor concentration in the space charge region, ε_{SC} = 8.9[39] is the dielectric constant of GaN, and other constants have their common meaning. The data presented in Figure 3b were fitted with the carrier concentration determined by Hall measurements, $N_D = 1.5 \times 10^{19}$ cm⁻³. The clear shift in the

Table 1. Summary of the impedance parameters obtained in this study for various systems.

	C_P[a)] [μFcm^{-2}]	U_{FB}[b)] [V]
Ni^{2+}-loaded	0.65 ± 0.02	− 1.92 ± 0.30
Unloaded (EDTA)	0.88 ± 0.02	− 1.11 ± 0.18
eGFP-loaded	0.78 ± 0.02	− 1.48 ± 0.09

[a)]Measured at U_{Bias} = 200 mV in order to show the data which are definitely situated in the linear part of the Mott-Schottky plot; [b)]Calculated from the experiments at 0 mV ≤U_{Bias} ≤ 900 mV. To confirm the reproducibility and the statistical reliability, three impedance spectra were measured at each bias potential, and four independently prepared samples were used. Though the absolute values in C_P shows slight deviations (within 10%), this lies within the difference in the C_P of bare GaN electrodes in electrolyte.

respective Mott-Schottky plots implies a distinct change in the flat band potential.

As presented in **Table 1** and **Figure 4**a, the interface capacitance was C_P = 0.65 μFcm^{-2}, when NTA lipids were loaded with Ni^{2+} (red). The exchange to EDTA buffer (blue) led to a clear

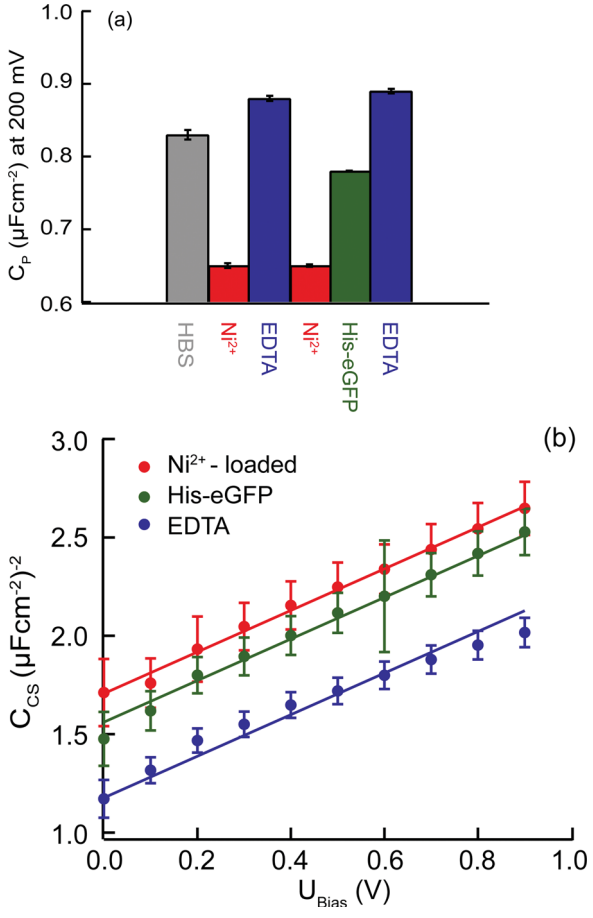

Figure 4. Switching of (a) interface capacitance C_P and (b) flat band potential U_{FB} according to membrane preparation (grey) → loading with Ni^{2+} (red) → unloading with EDTA (blue) → re-loading with Ni^{2+} (red) → loading with eGFP (green) → unloading with EDTA (blue) of the 2 mol% DOGS-NTA containing membrane. Three different levels presented in Scheme 1 are clearly distinguishable.

increase to C_P = 0.88 μFcm^{-2}. It should be noted that the capacitance value returned exactly to the former level upon a second loading with Ni^{2+}. The experiments at various bias potentials implied a clear switching of the flat band potentials between Ni^{2+}-loaded state and unloaded state, $U_{FB(Ni)}$ = − 1.92 V and $U_{FB(unloaded)}$ = −1.11 V, respectively (Figure 4b). The change in the flat band potential due to the unloading of NTA groups by EDTA buffer ΔU_{FB} = 0.81 V can be attributed to the change in net charges in NTA group (Scheme 1). By assuming the area per lipid molecule in the fluid phase of about 0.65 nm^2[40] and considering the amount of charged lipid DOGS-NTA to be 2 mol% and the change in the molecular net charge by 1 e$^-$, the corresponding change in surface charge density can be estimated to be $\Delta Q = 0.5 \times 10^{-6}$ Ccm^{-2}.

The docking of his-eGFP proteins (0.25 μgmL^{-1}) to Ni^{2+}-loaded NTA groups led to a distinct change in the interface capacitance C_P = 0.78 μFcm^{-2}, corresponding to a flat band potential of $U_{FB(eGFP)}$ = −1.48 V.

As reported previously,[41] the isoelectric point of his-eGFP is ~4.8–5.0, suggesting that his-eGFP is negatively charged at pH = 7.5. The decrease in U_{FB} caused by the docking of his-eGFP to Ni^{2+}-loaded NTA groups (ΔU_{FB} ~ 0.44 mV) is plausible if one considers the negative net charges carried by his-eGFP. It should be noted that all changes in the impedance spectra are fully reversible at 0 mV ≤ U_{bias} ≤ 900 mV, verifying the electrochemical stability and reproducibility of the EIS set up. Moreover, control experiments confirmed that the buffer exchange in the absence of lipid monolayer caused no changes in both C_{CS} and U_{FB} (Supporting Information S3).

The switching between the three states (Ni^{2+}-loaded, eGFP-loaded, and EDTA) can be also discriminated even at 0.5 mol% DOGS-NTA containing monolayer (Supporting Information S4). The obtained results demonstrate that the change in membrane surface charge density of ΔQ = 0.1 μC/cm^2, which corresponds to a change of one elementary charge per 130 nm^2, can be detected using the membrane-based EIS system on GaN. In fact, the sensitivity achieved here with GaN as the semiconductor material is better than the one on ITO (ΔQ = 2.2 μC/cm^2)[22] and GaAs (ΔQ = 0.9 μC/cm^2).[32] It should be pointed out that the docking of recombinant proteins has firstly been detected in this study, suggesting a large potential of membrane-based EIS sensors on GaN semiconductors.

It should be noticed that the excellent chemical robustness of GaN allows for the stable operation of the membrane EIS sensors over weeks, which could not be reached by other compound semiconductors. Furthermore, the reproducible switching of the electrochemical properties ensures the stability and reliability of the membrane voltmeter on GaN.

In order to demonstrate the potential of this work we highlight the possibility of an optical readout of the membrane-based charge sensor using optically active InGaN/GaN quantum dot (QD) structures (i.e. InGaN QDs embedded in GaN matrix material)[21] as optically active substrates with chemically identical surface properties as the *n*-GaN electrodes. These quantum structures provide a room temperature photoluminescence (PL) signal whose intensity is highly sensitive to variations in the surface potential (cf. **Figure 5**.)[21] As preliminary test of this approach InGaN/GaN QD transducers were functionalized with DOGS-NTA using the methods described

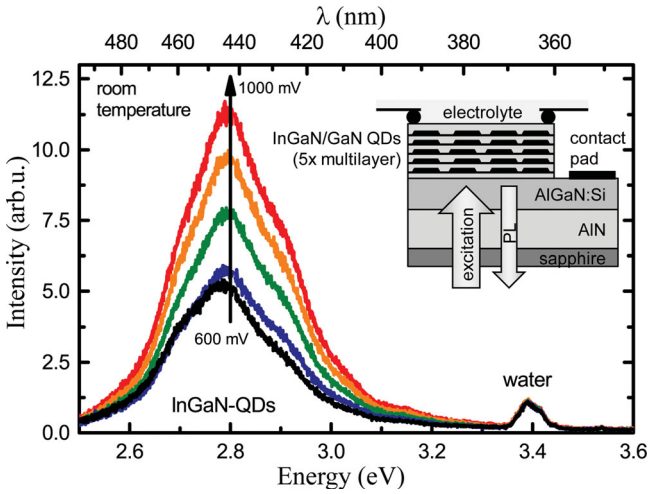

Figure 5. Room-temperature PL spectra of InGaN/GaN quantum dot transducers under applied bias between 600 mV and 1000 mV (in steps of 100 mV). The insert shows a schematic of the transducer structure featuring five InGaN-QD layers embedded in GaN matrix grown on a highly conductive AlGaN:Si backside contact layer. The transducer surface is in contact with the electrolyte and the device is operated in three-electrode configuration. Excitation and detection of the charge dependent PL signal takes place from the sample's backside.

above. **Figure 6** shows three PL spectra of the hybrid system in different charging states. The InGaN-QD related PL signal at 2.78 eV showed a higher intensity in the Ni^{2+}-loaded state than in pure HEPES buffer solution (unloaded state). After EDTA addition (intentional unloading) the PL intensity returned to its original value in agreement with the results shown for the flat band voltage in Figure 4b. Hence, the group III-nitride material system offers the attractive possibility for membrane-based charge sensing with optical readout.

3. Conclusion

We demonstrated that supported lipid monolayers deposited on wide band-gap gallium nitride (GaN) electrodes can be used as a membrane-based electrolyte-insulator-semiconductor (EIS) sensor platform. Owing to the excellent chemical/electrochemical stability of GaN under various bias potentials and wide frequency windows, changes in the surface charge density due to the reversible complexation/de-complexation of chelator (NTA) lipids and the binding/unbinding of histidine-tagged fusion proteins can be detected with an accuracy of ΔQ = 0.1 μC/cm^2. Furthermore, the reproducible switching of surface charges could be observed for more than a week of experiment, which ensures the stability and reliability of supported lipid monolayers on chemically robust GaN. Taking the advantage of wide bad-gap semiconductors, we examined the potential of optically active InGaN/GaN quantum dot (QD) structures, consisting of 5 InGaN QD layers embedded in GaN matrix, as an optical sensor platform to detect changes in the surface potential from the intensity of photoluminescence signals at room temperature.

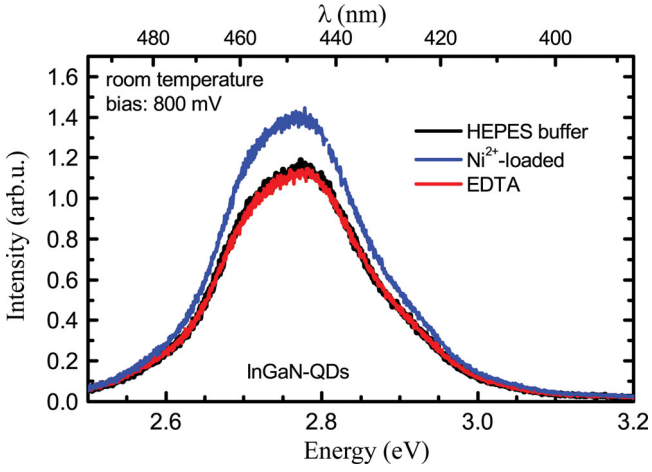

Figure 6. PL spectra of InGaN/GaN quantum dot transducers functionalized with DOGS-NTA under different charging states.

4. Experimental Section

Gallium Nitride Substrates: GaN films with (0001)-orientation grown on c-plane sapphire substrates (330 μm) with a total thickness of 3 μm (first low temperature undoped GaN buffer, possibly recrystallized, 0.3 μm; then GaN: C-compensated, 2.7 μm) were used as electrode material. GaN electrodes were grown by metal organic chemical vapor deposition (MOCVD) (TopGaN Ltd, Warsaw, Poland). A 210 nm thick Si-doped (2×10^{19} cm^{-3}) GaN film was deposited to ensure a sufficiently high semiconductor space charge capacitance for electrochemical sensing.

Chemicals: Cholesterol and 1,2-dioleoyl-*sn*-glycero-3-[(*N*-(5-amino-1-carboxypentyl)iminodiacetic acid)succinyl] (nickel salt) (DOGS-NTA(Ni)) were purchased from Avanti Polar Lipids Inc. (Alabaster, AL, USA). Dimyristoylphosphatidylcholine (DMPC) was a generous gift from Lipoid GmbH (Ludwigshafen, Germany). HEPES [4-(2-hydroxyethyl) piperazine-1-ethanesulfonic acid] was purchased from Carl Roth GmbH (Karlsruhe, Germany), $NiCl_2$ was purchased from Sigma Aldrich Chemie (Steinheim, Germany). All other chemicals were purchased from Appli Chem (Darmstadt, Germany) and were used without further purification.

The standard HEPES buffered saline (HBS) buffer was prepared using 10 mM HEPES and 80 mM NaCl. For the reversible charging of chelator lipids, HBS buffers (pH 7.5) containing either 1 mM $NiCl_2$ (Nickel buffer) and 80 mM NaCl or 100 mM EDTA (disodium salt dehydrate) (ethylenediaminetetraacetate, EDTA buffer) were used. All buffers were titrated with NaOH to pH 7.5 and degassed prior to use.

The plasmid used for GFP expression was derived from the pQE31-GFP-CBP vector[42] by deletion of the C-terminal CBP sequence. This plasmid was a kind gift obtained from Dr. Ingrid M. Weiss, Universität Regensburg, Germany.

Sample Preparation: Prior to the surface functionalization, the samples were cleaned according to the modified RCA cleaning procedure.[43] First, they were immersed and sonicated with acetone, ethanol and methanol, then sonicated in a freshly prepared solution of 1:1:5 (v/v) H_2O_2 (30%)/NH_4OH (30%)/H_2O for 5 min and kept for another 45 min at 60 °C to achieve hydrophilic surfaces. Finally, they were rinsed 10 times with water, thoroughly dried at 70 °C and stored in a vacuum chamber.

To achieve hydrophobic surfaces, GaN substrates were silanized with octadecyltrimethoxysilane (ODTMS).[18,44] The reaction was performed using 60 min sonication in a 5% (v/v) solution of ODTMS in constantly ice-cooled (T = 0 °C),[45] water-free toluene with 0.5% (v/v) butylamine as a catalyst. Subsequently, the substrates were incubated for another 30 min without sonication at T = 0 °C. To remove physisorbed silanes from the sample surface, the samples were rinsed and sonicated in toluene and ethanol for 2 min. Finally, they were dried at 70 °C and stored in a vacuum chamber. The quality of each ODTMS monolayer

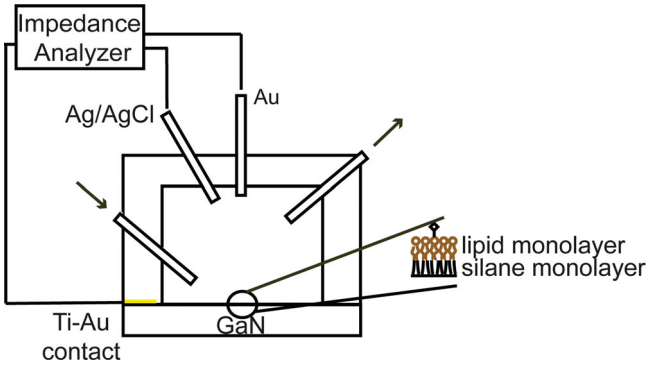

Scheme 2. Schematic illustration of the electrochemical cell used in this study. The functionalized GaN is used as a work electrode, Ag/AgCl and Pt as a reference and counter electrodes, respectively.

was checked by a static contact angle measurement in sessile drop configuration. A water contact angle of beyond 90° confirmed that the GaN surface was hydrophobic enough for the deposition of a lipid monolayer.

A lipid monolayer was deposited on freshly silanized GaN by fusion of DMPC vesicles, containing 35 mol% cholesterol[10b] and 2 mol% or 0.5 mol% DOGS-NTA(Ni). The lipid suspension was incubated at room temperature overnight and the supported lipid monolayer was washed with the standard HBS buffer to remove the unbound vesicles.

Electrochemical Methods: The electrochemical properties of the GaN electrodes functionalized with supported membranes were determined using electrochemical impedance spectroscopy over a wide frequency range between 50 mHz and 50 kHz (VoltaLab 40, Radiometer Analytical, Lyon, France) inside a Faraday cage. Spectra were acquired with an AC amplitude of 20 mV at bias potentials between 0 and 900 mV. A 750 Ω resistance was inserted in series with the GaN electrode to improve the high-frequency signal. Electrochemical measurements were carried out in an electrochemical flow chamber equipped with three electrodes. The setup, represented in **Scheme 2**, consisted of a GaN work electrode, a Pt counter electrode and a Ag/AgCl reference electrode (World Precision Instruments, Berlin, Germany). Due to the insulating sapphire carrier substrate, the GaN electrodes were contacted from outside the chamber through four copper plates touching the front side corners of the substrate with four Ti (30 nm)/Au (100 nm) Ohmic contacts. An O-ring prevented leakage of the buffer solution out of the chamber and defined an active electrode area of 0.5 cm^2. To avoid the formation of dielectric surface layers, the buffer was continuously pumped through the chamber by a peristaltic pump (Perimax, Spetec GmbH, Erding, Germany).

Atomic Force Microscopy (AFM): All measurements were performed in contact mode with a JPK Nanowizard 3 (JPK Instruments AG, Berlin, Germany) using Sharp Nitride Lever SNL-10 cantilevers with a spring constant of $k = 0.35$ N/m and a tip radius of <12 nm (Bruker, Germany). The scan rate was set to be 0.5 Hz for scan areas between 1×1 μm^2 and 10×10 μm^2.

Fluorescence Recovery after Photobleaching (FRAP): The measurements were carried out on Perkin Elmer ERS-6 (Nikon TE2000 inverted microscope, Nikon Plan Apo VC 60× NA 1.4 oil immersion objective, Hamamatsu C9100–02 EMCCD camera) at Nikon Imaging Center, Heidelberg University. The spot size was r = 4.47 µm. The data were evaluated according to the procedure described by Soumpasis.[46]

InGaN/GaN Quantum Dot Substrates: Polar InGaN/GaN quantum dot (QD) multilayers, consisting of 5 InGaN QD layers embedded in GaN matrix, were grown by plasma-assisted molecular beam epitaxy on (0001)-oriented AlN-on-sapphire templates.[47] The surface properties of the QD structures are chemically identical to those of the *n*-GaN electrodes. The In concentration in the QDs was estimated to ~10%.[21] A conductive Si-doped $Al_{0.35}Ga_{0.65}N$ intermediate layer (thickness 500 nm-700 nm) acts as a backside contact for the QD stack (cf. inset of Figure 5 for a schematic of the sample structure). The AlGaN back contact layer was opened at the edges of the sample by photolithography and Ar ion-beam etching; Ohmic contacts were realized by deposition of a Ti/Au (25 nm/120 nm) metallization.

Photoluminescence Measurements: Photoluminescence (PL) measurements in liquid environment were performed in a flow chamber using the QD sample as a window for backside excitation and detection. The chamber was equipped with a three-electrode setup using the AlGaN contact layer as working electrode, a Pt counter electrode, and an Ag/AgCl reference electrode in order to define the optical transducer's electrochemical working point.[21] PL excitation was carried out from the sample backside with the 325 nm line of a HeCd laser focused by a 10× objective resulting in a laser spot diameter of the order of 20 µm. The PL signal was collected by the same objective, dispersed in a spectrometer (focal length of 250 mm and 3600 lines/mm grating) and detected by a CCD camera. Figure 5 depicts PL spectra recorded in contact with HEPES buffer and at different cathodic bias values. The spectra show a QD-related emission at 2.8 eV (440 nm) and an emission at 3.4 eV (365 nm) attributed to the intrinsic luminescence of water occurring under UV excitation.[48] The intensity of the QD-related PL is highly sensitive to variations in the surface potential featuring an increasing intensity under cathodic bias due to the suppression of non-radiative loss mechanisms.[21] For experiments with functionalized transducer surfaces the bias is adjusted to 800 mV for maximum sensitivity.

Supporting Information

Supporting Information is available from the Wiley Online Library or from the author.

Acknowledgements

This work was supported by the German Federal Ministry of Education and Research (BMBF, 13N9111), Helmholtz Program "BioInterface", and the Deutsche Forschungsgemeinschaft (DFG, Ei 518/5). N.F. thanks to the Studienstiftung des deutschen Volkes e.V. for support. M.T. is a member of the German Excellence Cluster "Cell Network". iCeMS is supported by World Premier International Research Center Initiative (WPI), MEXT, Japan.

Received: February 4, 2014
Revised: March 13, 2014
Published online: May 13, 2014

[1] P. Bergveld, *Biosensors* **1986**, *2*, 15–34.
[2] a) E. Sackmann, *Science* **1996**, *271*, 43–48; b) E. Sackmann, M. Tanaka, *Trends Biotechnol.* **2000**, *18*, 58–64.
[3] a) Y. Cui, Q. Q. Wei, H. K. Park, C. M. Lieber, *Science* **2001**, *293*, 1289–1292; b) F. Patolsky, G. F. Zheng, C. M. Lieber, *Anal. Chem.* **2006**, *78*, 4260–4269.
[4] E. Katz, I. Willner, *ChemPhysChem* **2004**, *5*, 1084–1104.
[5] a) S. M. Luber, K. Adlkofer, U. Rant, A. Ulman, A. Golzhauser, M. Grunze, D. Schuh, A. Tanaka, M. Tornow, G. Abstreiter, *Physica E* **2004**, *21*, 1111–1115; b) G. Steinhoff, B. Baur, G. Wrobel, S. Ingebrandt, A. Offenhausser, A. Dadgar, A. Krost, M. Stutzmann, M. Eickhoff, *Appl. Phys. Lett.* **2005**, *86*, 033901; c) G. Steinhoff, M. Hermann, W. J. Schaff, L. F. Eastman, M. Stutzmann, M. Eickhoff, *Appl. Phys. Lett.* **2003**, *83*, 177–179.
[6] G. Horowitz, *J. Mater. Res.* **2004**, *19*, 1946–1962.
[7] a) T. Sauer, W. Caseri, G. W. A. Vogel, B. Hoffmann, *J. Phys. D: Appl. Phys.* **1990**, *23*, 79–84; b) A. Vogel, B. Hoffmann, T. Sauer, G. Wegner, *Sens. Actuat. B* **1990**, *1*, 408–411.
[8] M. Ben Ali, R. Kalfat, H. Sfihi, J. M. Chovelon, H. Ben Ouada, N. Jaffrezic-Renault, *Sens. Actuat. B* **2000**, *62*, 233–237.

[9] R. J. Mortimer, A. Beech, *J. Electrochem. Soc.* **2000**, *147*, 780–786.
[10] a) S. Gritsch, P. Nollert, F. Jahnig, E. Sackmann, *Langmuir* **1998**, *14*, 3118–3125; b) O. Purrucker, H. Hillebrandt, K. Adlkofer, M. Tanaka, *Electrochim. Acta* **2001**, *47*, 791–798.
[11] H. Hillebrandt, G. Wiegand, M. Tanaka, E. Sackmann, *Langmuir* **1999**, *15*, 8451–8459.
[12] a) J. Nissen, S. Gritsch, G. Wiegand, J. O. Radler, *Eur. Phys. J. B* **1999**, *10*, 335–344; b) M. Tanaka, F. Rehfeldt, M. F. Schneider, G. Mathe, A. Albersdörfer, K. R. Neumaier, O. Purrucker, E. Sackmann, *J. Phys.: Condens. Matter* **2005**, *17*, 649–663.
[13] a) B. Raguse, V. Braach-Maksvytis, B. A. Cornell, L. G. King, P. D. J. Osman, R. J. Pace, L. Wieczorek, *Langmuir* **1998**, *14*, 648–659; b) C. Steinem, A. Janshoff, H. J. Galla, M. Sieber, *Bioelectrochem. Bioenerg.* **1997**, *42*, 213–220.
[14] E. Sackmann, *Biological Membranes Architecture and Function. Handbook of Biological Physics*, Vol. *1* (Eds: R. Lipowsky, E. Sackmann), Elsevier Science, New York **1995**, Ch. 1.
[15] P. Fromherz, *ChemPhysChem* **2002**, *3*, 276–284.
[16] M. Tutus, O. Purrucker, Y. Adlkofer, M. Eickhoff, M. Tanaka, *Phys. Status Solidi B* **2005**, *242*, 2838–2845.
[17] a) S. Schaefer, A. H. R. Koch, A. Cavallini, M. Stutzmann, I. D. Sharp, *J. Phys. Chem. C* **2012**, *116*, 22281–22286; b) G. Steinhoff, O. Purrucker, M. Tanaka, M. Stutzmann, M. Eickhoff, *Adv. Funct. Mater.* **2003**, *13*, 841–846.
[18] B. Baur, J. Howgate, H. G. von Ribbeck, Y. Gawlina, V. Bandalo, G. Steinhoff, M. Stutzmann, M. Eickhoff, *Appl. Phys. Lett.* **2006**, *89*, 183901.
[19] T. Schubert, G. Steinhoff, H. G. von Ribbeck, M. Stutzmannn, M. Eickhoff, M. Tanaka, *Eur. Phys. J. E* **2009**, *30*, 233–238.
[20] R. Stine, B. S. Simpkins, S. P. Mulvaney, L. J. Whitman, C. R. Tamanaha, *Appl. Surf. Sci.* **2010**, *256*, 4171–4175.
[21] J. Teubert, S. Koslowski, S. Lippert, M. Schaefer, J. Wallys, G. Dimitrakopulos, T. Kehagias, P. Komninou, A. Das, E. Monroy, M. Eickhoff, *J. Appl. Phys.* **2013**, *114*, 074313.
[22] H. Hillebrandt, M. Tanaka, E. Sackmann, *J. Phys. Chem. B* **2002**, *106*, 477–486.
[23] a) H. Gerischer, W. Mindt, *Electrochim. Acta* **1968**, *13*, 1329–1341; b) G. Horowitz, P. Allongue, H. Cachet, *J. Electrochem. Soc.* **1984**, *131*, 2563–2569.
[24] A. J. Bard, L. R. Faulkner, *Electrochemical Methods – Fundamentals and Applications*, John Wiley & Sons, New York **1980**.
[25] K. Adlkofer, M. Tanaka, *Langmuir* **2001**, *17*, 4267–4273.
[26] P. Schmuki, H. Böhni, J. A. Bardwell, *J. Electrochem. Soc.* **1995***142*, 1705–1712.
[27] P. Allongue, H. Cachet, *J. Electrochem. Soc.* **1985**, *132*, 45–52.
[28] K. Adlkofer, M. Tanaka, H. Hillebrandt, G. Wiegand, E. Sackmann, T. Bolom, R. Deutschmann, G. Abstreiter, *Appl. Phys. Lett.* **2000**, *76*, 3313–3315.
[29] a) K. Adlkofer, W. Eck, M. Grunze, M. Tanaka, *J. Phys. Chem. B* **2003**, *107*, 587–591; b) A. Shaporenko, K. Adlkofer, L. S. O. Johansson, M. Tanaka, M. Zharnikov, *Langmuir* **2003**, *19*, 4992–4998.
[30] H. Hillebrandt, M. Tanaka, *J. Phys. Chem. B* **2001**, *105*, 4270–4276.
[31] J. E. B. Randles, *Discuss. Faraday Soc.* **1947**, *1*, 11–19.
[32] D. Gassull, A. Ulman, M. Grunze, M. Tanaka, *J. Phys. Chem. B* **2008**, *112*, 5736–5741.
[33] D. Axelrod, D. E. Koppel, J. Schlessinger, E. Elson, W. W. Webb, *Biophys. J.* **1976**, *16*, 1055–1069.
[34] H. Sigl, G. Brink, M. Seufert, M. Schulz, G. Wegner, E. Sackmann, *Eur. Biophys. J.* **1997**, *25*, 249–259.
[35] A. L. Beauchamp, J. Israeli, H. Saulnier, *Can. J. Chem.* **1969**, *47*, 1269–1273.
[36] L. Schmitt, C. Dietrich, R. Tampe, *J. Am. Chem. Soc.* **1994**, *116*, 8485–8491.
[37] a) M. Tanaka, *MRS Bull.* **2006**, *31*, 513; b) M. Tanaka, E. Sackmann, *Nature* **2005**, *437*, 656–663.
[38] a) F. Cardon, W. P. Gomes, *J. Phys. D: Appl. Phys.* **1978**, *11*, L63; b) W. P. Gomes, F. Cardon, *Prog. Surf. Sci.* **1982**, *12*, 155–215.
[39] M. E. Levinshtein, S. L. Rumyantsev, M. S. Shur, *Properties of Advanced SemiconductorMaterials GaN, AlN, InN, BN, SiC, SiGe* (Eds: M. E. Levinshtein, S. L. Rumyantsev, M. S. Shur), John Wiley & Sons, Inc., UK **2001**, pp.1–30.
[40] G. Lantzsch, H. Binder, H. Heerklotz, M. Wendling, G. Klose, *Biophys. Chem.* **1996**, *58*, 289–302.
[41] M. Tanaka, J. Hermann, I. Haase, M. Fischer, S. G. Boxer, *Langmuir* **2007**, *23*, 5638–5644.
[42] I. M. Weiss, V. Schonitzer, *J. Struct. Biol.* **2006**, *153*, 264–277.
[43] W. Kern, D. Puotinen, *RCA Review* **1970**, *31*, 187–206.
[44] a) J. F. Mooney, A. J. Hunt, J. R. McIntosh, C. A. Liberko, D. M. Walba, C. T. Rogers, *Proc. Natl. Acad. Sci. USA* **1996**, *93*, 12287–12291; b) J. Howgate, S. J. Schoell, M. Hoeb, W. Steins, B. Baur, S. Hertrich, B. Nickel, I. D. Sharp, M. Stutzmann, M. Eickhoff, *Adv. Mater.* **2010**, *22*, 2632–2636.
[45] a) J. B. Brzoska, N. Shahidzadeh, F. Rondelez, *Nature* **1992**, *360*, 719–721; b) A. N. Parikh, D. L. Allara, I. B. Azouz, F. Rondelez, *J. Phys. Chem.* **1994**, *98*, 7577–7590.
[46] D. M. Soumpasis, *Biophys. J.* **1983**, *41*, 95–98.
[47] A. Das, P. Sinha, Y. Kotsar, P. K. Kandaswamy, G. P. Dimitrakopulos, T. Kehagias, P. Komninou, G. Nataf, P. De Mierry, E. Monroy, *J. Cryst. Growth* **2011**, *323*, 161–163.
[48] V. I. Lobyshev, R. E. Shikhlinskaya, B. D. Ryzhikov, *J. Mol. Liq.* **1999**, *82*, 73–81.